

Shortcut to adiabaticity in a Stern-Gerlach apparatusFrançois Impens¹ and David Guéry-Odelin²¹*Instituto de Física, Universidade Federal do Rio de Janeiro, Rio de Janeiro, RJ 21941-972, Brazil*²*Laboratoire Collisions, Agrégats, Réactivité, IRSAMC, Université de Toulouse, CNRS, UPS, Toulouse, France*

(Received 13 July 2017; published 12 October 2017)

We show that the performances of a Stern-Gerlach apparatus can be improved by using a magnetic field profile for the atomic spin evolution designed with the shortcut-to-adiabaticity technique. Interestingly, it can be made more compact, for atomic beams propagating at a given velocity, and more resilient to a dispersion in velocity in comparison with the results obtained with a standard uniform rotation of the magnetic field. Our results are obtained using a reverse-engineering approach based on Lewis-Riesenfeld invariants. We discuss quantitatively the advantages offered by our configuration in terms of the resources involved and show that it drastically enhances the fidelity of the quantum state transfer achieved by the Stern-Gerlach device.

DOI: [10.1103/PhysRevA.96.043609](https://doi.org/10.1103/PhysRevA.96.043609)**I. INTRODUCTION**

The Stern-Gerlach apparatus, used in the last century to obtain experimental evidence of angular momentum quantization [1], also has interesting features for atom optics [2]. In particular, this device has been used successfully in the first observation of a geometric phase [3] in atom interferometry [4]. This system entangles the external atomic motion with the total angular atomic momentum and produces a spatial separation between atomic wave packets corresponding to different angular momenta. The Stern-Gerlach device can be used to perform transformations on the atomic spins, mapping initial angular momentum states to determined final states.

These transformations are usually achieved with a magnetic field presenting a helicoidal profile [5]. A simple way to map reliably initial spin states to well-defined target spin states is to design the magnetic field profile in such a way that the atomic spin follows the locally rotating magnetic field adiabatically in the course of its propagation through the device. The bottleneck of this approach is that the adiabatic regime imposes a minimum length over which the magnetic field may change its direction. This length is proportional to the atomic velocity and inversely proportional to the magnetic field modulus. Since strong magnetic fields may be undesirable, there is a trade-off between the speed of the adiabatic evolution and the magnetic field strength.

The purpose of this article is to show that this trade-off can be greatly improved by using the shortcut-to-adiabaticity (STA) technique [6]. More precisely, we design a suitable magnetic field profile by using the reverse-engineering approach based on the Lewis-Riesenfeld invariants [7–9]. These methods enable one to guarantee a transitionless evolution faster than the time scale imposed by the adiabatic regime. The STA approach has been shown experimentally to efficiently speed up the transport or manipulation of wave functions [10–17] and even thermodynamical transformations [18–20]. Concerning the transfer of quantum states, recent impressive implementations have been reported in cold-atom experiments [21], solid-state architectures [22], and optomechanical systems [23]. The transposition of those ideas to integrated optics devices has been recently explored [24–26].

Our proposal of a STA-engineered Stern-Gerlach device outperforms the traditional rotating field in terms of the speed

of the quantum evolution for a given amount of resources, here the magnetic field. The STA-engineered Stern-Gerlach device is also robust toward a dispersion in the atomic velocities and may achieve very high fidelities in an atomic spin-state transfer. We will illustrate our arguments by considering specifically the case of spin-1 particles such as the hydrogen fragments issued from H₂ dissociation [27–29]. This example is relevant since an experiment based on an arrangement of Stern-Gerlach devices has been recently proposed to evaluate the spin coherence of this dissociation [30].

The paper is organized as follows. In Sec. II, we investigate the efficiency of a Stern-Gerlach device using a plain helicoidal configuration of the magnetic field. In Sec. III, we provide the general framework to determine a suitable magnetic field in a Stern-Gerlach device using the STA technique. In Sec. IV, we study an example of such a magnetic field profile suitable to realize fast and robust angular momentum evolution. In particular, we estimate the quantum fidelity and the speedup of the spin transfer enabled by this configuration. We also study the resilience toward a dispersion in the atomic propagation times and compare the performance of this configuration with respect to a standard Stern-Gerlach apparatus using an equivalent magnetic field.

II. EFFICIENCY OF A STERN-GERLACH DEVICE WITH A HELICOIDAL MAGNETIC FIELD

In this section, we review the propagation of a spin-1 particle in a standard Stern-Gerlach device. This apparatus involves a helicoidal magnetic field which rotates at an angle of $\pi/2$ over a certain length, corresponding to a propagation time T for a given class of atomic velocities. An atom propagating at constant velocity along the helicoid axis experiences locally a uniform rotation of the magnetic field. We investigate the transfer of the angular momentum from the initial state $|J = 1, m_z = 1\rangle$ to the target state $|J = 1, m_x = 1\rangle$ as a function of the atomic propagation time T .

For this purpose, the particle is subjected to the time-dependent Hamiltonian $\hat{H}(\mathbf{B}(t)) = -\gamma \mathbf{B}(t) \cdot \hat{\mathbf{J}}$ between the initial time $t = 0$ and final time $t = T$. $\hat{\mathbf{J}}$ is the vectorial angular momentum operator of a spin-1 particle, and γ accounts for the strength of the coupling and includes the

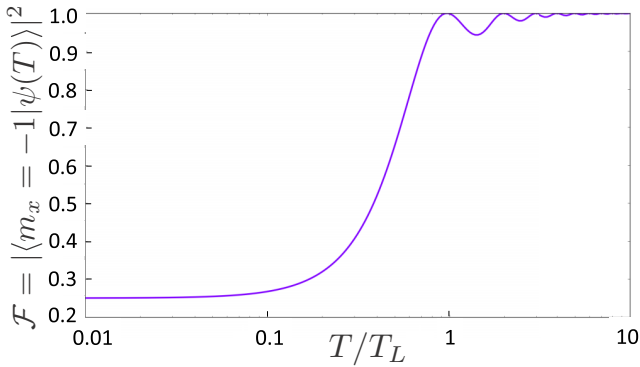


FIG. 1. Fidelity of the final state $\mathcal{F} = |\langle m_x = 1 | \psi(T) \rangle|^2$ as a function of the ratio T/T_L between the total time and the Larmor time. This profile is independent of the considered Larmor pulsation, which has been set to $\omega_L = 10^6$ rad/s in the numerical simulation.

atomic Landé factor. The magnetic field $\mathbf{B}(t)$ in the comoving frame seen at the central atomic position [31] reads $\mathbf{B}_{\text{st}}(t) = \text{Re}[B_0(\hat{\mathbf{z}} + i\hat{\mathbf{x}})e^{i\frac{\pi}{2}\frac{t}{T_L}}]$. As there is only a single characteristic time scale, namely, the Larmor time $T_L = 2\pi/\gamma B_0$ associated with the spin precession in the magnetic field, the efficiency of the quantum transfer may depend only on the ratio T/T_L . We have used the QUTIP package [32,33] to simulate the evolution of the initial spin state $|m_z = 1\rangle$ in a time-dependent rotating magnetic field. The efficiency of the spin transfer is quantified by the fidelity \mathcal{F} [34] of the final state $|\psi(T)\rangle$ to the target state $\mathcal{F} = |\langle m_x = 1 | \psi(T) \rangle|^2$.

The results are shown in Fig. 1. For short durations $T \ll T_L$, the fidelity of the final state is barely higher than that of the initial state. As expected, in this limit, the atomic angular momentum state is almost unaffected by the Stern-Gerlach device: the rotation of the magnetic field is too fast to drive the atomic spin. On the other hand, for times $T \gg T_L$, the atomic spin follows adiabatically the field, yielding a final state very close to the target state. A quantum fidelity equal to unity is achieved when $T = T_L$. For total times T greater or equal to a few Larmor times T_L , the fidelity stays higher than 99%. The Larmor time T_L , which is inversely proportional to the strength of the magnetic field, thus corresponds to a reliable spin transfer in a standard Stern-Gerlach apparatus. We shall use this duration to determine the figure of merit of a Stern-Gerlach device enhanced by the STA technique. Using typical experimental parameters for Stern-Gerlach atom interferometry with hydrogen fragments [4], we consider atomic velocities $v \sim 10$ km/s, a gyromagnetic ratio $\gamma \simeq \mu_b/\hbar$, a magnetic field $B_0 = 0.1$ G, and a Larmor time $\nu_L = 0.14$ MHz. The corresponding Larmor time $T_L \simeq 7 \mu\text{s}$ then yields the minimum length of a few $L \simeq 7$ cm for an efficient spin transfer in a Stern-Gerlach device with a helicoidal magnetic field.

Finally, we note that the fidelity is a nonmonotonic function of the ratio T/T_L . The small oscillations shown in Fig. 1 are consistent with the predictions for the spin transition amplitudes of atomic spins experiencing a nonadiabatic evolution in an inhomogeneous magnetic field [35], evidenced experimentally for metastable hydrogen atoms [36,37].

III. DETERMINATION OF THE MAGNETIC FIELD FROM LEWIS-RIESENFELD INVARIANTS

In this section, we search for a magnetic field profile suitable for realizing fast spin evolution of a spin-1 particle in a Stern-Gerlach device, with an initial angular momentum along the O_z axis and a target angular momentum state along the O_x axis. We find the general equations for the field and determine suitable boundary conditions to be satisfied by the Lewis-Riesenfeld invariants [7].

A. General equations for the dynamical invariant

For a given time-dependent Hamiltonian $\hat{H}(t)$, a dynamical invariant $\hat{I}(t)$ fulfills the equation [7]

$$i\hbar \frac{\partial \hat{I}(t)}{\partial t} = [\hat{H}(t), \hat{I}(t)]. \quad (1)$$

A natural choice for the rotation of a spin 1 is to search for a dynamical invariant in the form $\hat{I}(t) = \mathbf{u}(t) \cdot \mathbf{J}(t)$, where the spin operators $\{\hat{J}_k\}$, with $k = x, y, z$, form a closed Lie algebra [38,39] as the Pauli matrices for SU(2) and $\mathbf{u}(t)$ is a vector that needs to be determined. Interestingly, the dynamical operatorial equation (1) can be translated in a simple linear differential equation describing a clockwise precession of the vector $\mathbf{u}(t)$ around the magnetic field $\mathbf{B}(t)$,

$$\frac{d\mathbf{u}(t)}{dt} = \gamma \mathbf{u}(t) \times \mathbf{B}(t). \quad (2)$$

In the following, we set the evolution of $\mathbf{u}(t)$ and infer from Eq. (2) the explicit expression for $\mathbf{B}(t)$ [40]. This amounts to reverse engineering Eq. (2). Actually, we have a lot of freedom to choose the function $\mathbf{u}(t)$, and this choice does not fully constrain the function $\mathbf{B}(t)$. In what follows, we fix $B_y = 0$ and proceed to determine $\mathbf{B}(t)$ from Eq. (2) [41]. Finally, to connect the eigenstates at initial and final times of $\hat{I}(t)$ and $\hat{H}(t)$, we impose the following commutation relations: $[\hat{H}(0), \hat{I}(0)] = [\hat{H}(T), \hat{I}(T)] = 0$.

B. Resilience of the atomic spin transfer towards an atomic velocity dispersion

Before proceeding, we highlight an interesting property arising from the commutation between the invariant and Hamiltonian operators at the final time, i.e., $[\hat{H}(T), \hat{I}(T)] = 0$. From the equation of motion (1), this condition implies that $\frac{\partial \hat{I}}{\partial t}|_T = 0$. Consequently, to leading order, the eigenstates of the dynamical invariant $\hat{I}(T)$ are unaffected by a small fluctuation of the interaction time T with respect to a reference value T_0 . By construction, the atomic spin is an eigenstate of the invariant operator at all times. One thus expects that the final atomic spin state should also be unchanged to leading order by a small fluctuation of the atomic time of flight. This property enables one to perform an efficient spin rotation over a broad range of particle velocities, making the apparatus robust against an atomic velocity dispersion. In the next section, we will verify numerically this resilience of the spin transfer for a concrete example of magnetic field.

C. Relation between the magnetic field and dynamical invariant

The vector $\mathbf{u}(t)$ is conveniently parametrized in spherical coordinates as a unit vector, $\mathbf{u}(t) = (\sin \theta \cos \varphi, \sin \theta \sin \varphi, \cos \theta)$. From the precession equation (2), we get the components of the magnetic field as a function of the spherical angles $\theta(t)$ and $\varphi(t)$:

$$\gamma B_x(t) = \frac{\dot{\theta}}{\sin \varphi}, \quad \gamma B_z(t) = -\dot{\varphi} + \frac{\dot{\theta} \cos \theta \cos \varphi}{\sin \theta \sin \varphi}. \quad (3)$$

We shall thus search for acceptable angular functions avoiding divergences in the magnetic field. Typically, as seen from the equations above, such divergence may occur when the invariant pointer crosses the equatorial line defined by $\theta = 0$ or the meridians defined by $\varphi = 0, \pi$. This geometric constraint on the pointer trajectory sets a limit on the shortest spin-transfer time achievable with the STA method when using polynomial angles of a certain degree.

D. Boundary conditions on the spherical coordinates of the invariant

We derive here the boundary conditions to be fulfilled by the angular functions $(\theta(t), \varphi(t))$. These functions must enable the commutation between the invariant pointer and the Hamiltonian at the initial and final times. Since the initial and target states must be eigenvectors of the initial and final Hamiltonians, respectively, the magnetic field direction at these times is fixed according to $\mathbf{B}(0) = B_z^I \hat{z}$ and $\mathbf{B}(T) = B_x^F \hat{x}$. The commutation between the invariant and Hamiltonian is then ensured by setting the pointer $\mathbf{u}(t)$ parallel to the magnetic field at these times. This is achieved by imposing the following conditions on the spherical coordinates:

$$\begin{aligned} \theta(0) &= \pi, & \theta(T) &= \pi/2, \\ \varphi(0) &= \pi/2, & \varphi(T) &= 0. \end{aligned} \quad (4)$$

We now search for suitable expansions of the angular functions near the initial and final times that yield, through Eq. (3), the magnetic field $B_x(0) = 0$, $B_z(0) = B_z^I$ and $B_x(T) = B_x^F$, $B_z(T) = 0$. Using the perturbative expansion $\theta(t) = \pi + \alpha t^m + o(t^m)$ and $\varphi(t) = \pi/2 + \beta t^n + o(t^n)$ in the vicinity of $t = 0$, one obtains that the condition on the initial magnetic field is equivalent to $m > 1$, $n = 1$, and $\beta = -\gamma B_z^I / (m + n)$. The lowest-order expansion compatible with this condition corresponds to $n = 1$ and $m = 2$, that is, to say

$$\dot{\theta}(0) = 0, \quad \ddot{\theta}(0) > 0, \quad \dot{\varphi}(0) = -\gamma B_z^I / 3. \quad (5)$$

Using a similar expansion close to the final time with $\tau = t - T$, $\theta(\tau) = \pi/2 + \alpha' \tau^{m'} + o(\tau^{m'})$, and $\varphi(\tau) = \beta' \tau^{n'} + o(\tau^{n'})$ with $\tau = T - t$, one finds that the second set of conditions is equivalent to $m' = n' + 1$, $n' > 1$, and $m' \alpha' = \gamma \beta' B_x^F$. It can be fulfilled by choosing $n' = 2$ and $m' = 3$, yielding another set of conditions:

$$\begin{aligned} \varphi(T) &= 0, & \dot{\varphi}(T) &= 0, \\ \dot{\theta}(T) &= 0, & \ddot{\theta}(T) &= 0, & \ddot{\varphi}(T) &= \gamma B_x^F \dot{\varphi}(T). \end{aligned} \quad (6)$$

IV. EXAMPLE OF FAST MAGNETIC SPIN DRIVING WITH SHORTCUT TO ADIABATICITY

In this section, we give an example of a magnetic field profile realizing the STA by finding suitable polynomial functions for the spherical coordinates of the invariant pointer. We show by numerical simulations that this magnetic field profile yields an extremely reliable transfer of a single quantum state. We also discuss quantitatively the enhancement brought by the STA in a Stern-Gerlach device. For this purpose, one must consider the trade-off between the speedup brought by the STA and the amount of resources involved [23]. In contrast to the standard Stern-Gerlach device, the STA-engineered Stern-Gerlach involves a magnetic field with a time-dependent amplitude. To work out explicitly the comparison between the two devices, we shall consider as a resource either the average magnetic field seen by the atom in the STA device, i.e., $B_{\text{av}} = (1/T) \int_0^T dt \|\mathbf{B}(t)\|$, or the maximum magnetic field $B_{\text{max}} = \max\{\|\mathbf{B}(t)\|, t \in [0, T]\}$. These two criteria will provide different figures of merit. As seen below, with both criteria the STA-engineered Stern-Gerlach outperforms the standard device.

A. Example of suitable magnetic field profile

A simple way to match simultaneously the conditions (4), (5), and (6) is to look for polynomial functions of the form $\theta(t) = P(\frac{t}{T})$ and $\varphi(t) = Q(\frac{t}{T})$. Lowest-order suitable polynomials can be obtained as

$$\begin{aligned} P(x) &= \pi - 3\pi x^2 + 4\pi x^3 - \frac{3\pi}{2} x^4, \\ Q(x) &= \frac{\pi}{2} - \frac{B_z^I}{3} x + \left(-3\pi - \frac{6\pi}{B_x^F} + B_z^I\right) x^2 \\ &\quad + \left(4\pi + \frac{12\pi}{B_x^F} - B_z^I\right) x^3 + \left(-\frac{3\pi}{2} - \frac{6\pi}{B_x^F} + \frac{B_z^I}{3}\right) x^4, \end{aligned} \quad (7)$$

where we have introduced the adimensional magnetic fields $\vec{B}^I = \gamma T \mathbf{B}(0)$ and $\vec{B}^F = \gamma T \mathbf{B}(T)$. Let us stress that this choice of lowest-order polynomials is by no means unique since one of the relations constrains only the ratio of the time derivatives of the angular functions. With this choice, the azimuthal angle $\theta(t)$ of the field is completely independent of the initial and final values of the magnetic field, which affect the longitude angle $\varphi(t)$.

At this stage, one can determine the full magnetic field profile from Eq. (3). The values of the angle $\varphi(t)$ should be kept in the interval $]0, \pi[$ in order to avoid a divergence in the magnetic field [42]. For this purpose, one must choose carefully the sign of the magnetic field component B_x^F at the final time. Indeed, from Eq. (7) one has $\ddot{\theta}(T) < 0$, so by virtue of Eq. (6) one must have $B_x^F < 0$ to ensure that $\varphi(T) = 0$ is a local minimum. As a consequence of this choice, the considered device maps the initial state $|m_z = 1\rangle$ to the target spin state $|m_x = -1\rangle$. Figure 2 shows an example of a magnetic field profile determined by Eq. (7). For the considered parameters and with the propagation time $T = 2 \mu\text{s}$, an efficient

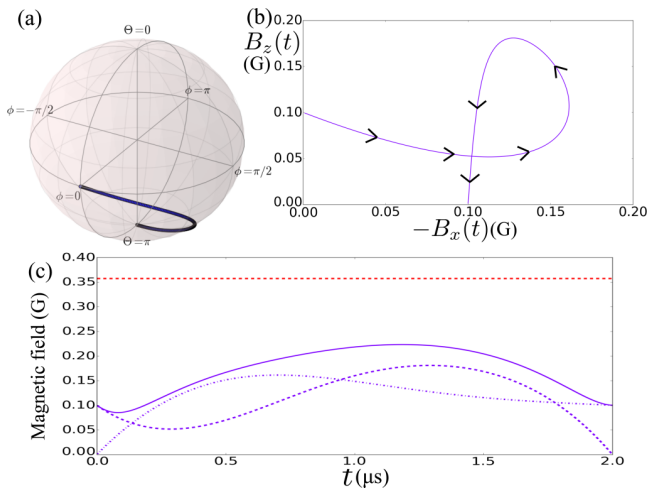


FIG. 2. Time-dependent magnetic field determined by reverse engineering with the Lewis-Riesenfeld invariant method for a total atomic propagation time $T = 2 \mu\text{s}$ and with the initial and final magnetic field components fixed to $B_z^I = 0.1 \text{ G}$ and $B_x^F = -0.1 \text{ G}$, respectively. (a) Trajectory of the pointer vector $\mathbf{u}(t)$ on the unit sphere. The initial point is on the pole and ending, and the final point is on the equator. (b) Parametric plot of the magnetic field seen at the atomic central position. (c) Plot of the norm $\|\mathbf{B}(t)\|$ (solid purple line) and the $-B_x(t)$ (dash-dotted purple line) and $B_z(t)$ (dotted purple line) components of the magnetic field as a function of time. The dashed red line represents the larger magnetic field B_{st}^0 enabling a reliable spin transfer in a standard device during the time T .

state transfer is achieved in a STA-enhanced Stern-Gerlach device with a maximum magnetic field $B_{\text{max}} \simeq 0.22 \text{ G}$ to be compared with the magnetic field $B_{\text{st}}^0 = 2\pi/\gamma T \simeq 0.36 \text{ G}$ required in a standard Stern-Gerlach device.

B. Fidelity and resilience of the spin transfer in a STA-engineered Stern-Gerlach device

Using the magnetic field defined in Eqs. (3), we simulate [32,33] the temporal evolution of an atomic spin in a Stern-Gerlach device with a STA-designed magnetic field. Precisely, we keep track of the expectation values of the angular momentum projections $\langle \hat{J}_z \rangle(t)$ and $\langle \hat{J}_x \rangle(t)$, as well as of the fidelity of the atomic spin state with respect to the target state $|m_x = -1\rangle$. The latter may be written as $\mathcal{F}(t) = |\langle m_x = -1 | \psi(t) \rangle|^2$, where the quantum state $|\psi(t)\rangle = \mathcal{T} \exp[-\frac{i}{\hbar} \int_0^t dt \hat{H}(\mathbf{B}(t))] |m_z = 1\rangle$ is the time-dependent atomic spin state evolved from the initial state $|m_z = 1\rangle$ through the interaction with the time-dependent magnetic field $\mathbf{B}(t)$.

The corresponding results are shown in Figs. 3 and 4, respectively. We first consider a STA Stern-Gerlach device and a standard Stern-Gerlach apparatus using equivalent magnetic fields. When the atomic spin propagates in a standard Stern-Gerlach device whose magnetic field is $B_{\text{av}} = (1/T) \int_0^T dt \|\mathbf{B}(t)\|$, the expectation value $\langle \hat{J}_x \rangle(T) > -1$ and the relatively low fidelity achieved ($\mathcal{F} \simeq 0.60$) reveal an imperfect transfer to the target state $|m_x = -1\rangle$. Even when the maximum field modulus B_{max} is used in the standard Stern-Gerlach device, the fidelity of the spin state to the target state

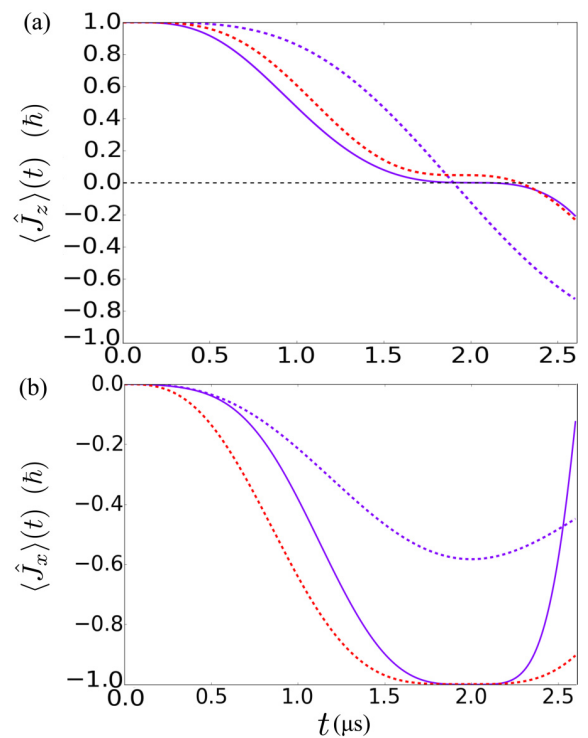


FIG. 3. Average values of the angular momentum projections (a) $\langle \hat{J}_z \rangle(t)$ and (b) $\langle \hat{J}_x \rangle(t)$ in units of \hbar as a function of the propagation time t . We consider the propagation in a STA-enhanced Stern-Gerlach device (solid purple lines) and in standard Stern-Gerlach devices using either a magnetic field equal to the temporal average of the STA magnetic field (dashed purple lines) or a larger magnetic field B_{st}^0 enabling an efficient spin transfer during the time $T = 2 \mu\text{s}$ (dashed red lines). Purple lines represent the use of equivalent resources in terms of magnetic field. The numerical parameters and magnetic fields are identical to those used in Fig. 2.

saturates at the value $\mathcal{F} \simeq 0.80$. In contrast, when the atomic spin propagates in the STA-designed magnetic field, the atomic spin projection expectation values are very close to $\langle \hat{J}_z \rangle(T) = 0$ and $\langle \hat{J}_x \rangle(T) = -1$, showing that the final spin state is very close to the target state $|m_x = -1\rangle$ at the final time T . With a standard Stern-Gerlach device using a larger magnetic field B_{st}^0 , one may achieve a good fidelity in the quantum state transfer over a large interval of propagation times t .

Nevertheless, the behavior of the fidelity near the optimal time is different for the standard and STA Stern-Gerlach devices, enabling the latter to reach very high fidelities in a single state transfer. Indeed, the error committed in this transfer $\epsilon(t) = 1 - \mathcal{F}(t)$ decreases sharply for the STA device and can become arbitrarily low in the vicinity of the ideal propagation time T . Differently, for the standard Stern-Gerlach device a finite error remains even at this ideal time. Its value depends on the magnetic field involved. In order to obtain a quantitative measure of the reliability of the spin transfer with a STA device, we analyze different fidelity thresholds for propagation times t close to the ideal time T . Denoting $\Delta t = t - T$ for the time propagation mismatch, the inset of Fig. 4 reveals that the error committed can be as low as $\epsilon(t) \leq 10^{-8}$ for

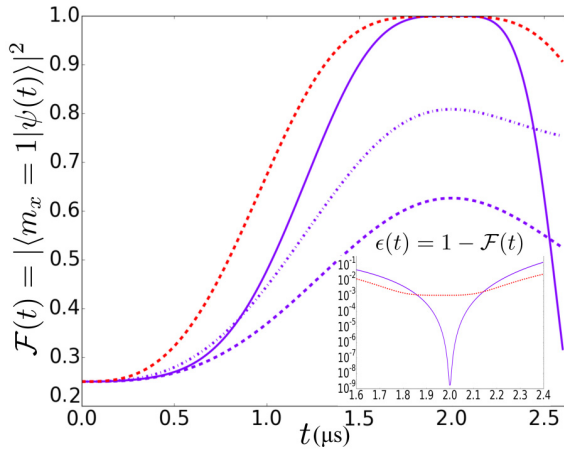


FIG. 4. Fidelity of the atomic spin state during its propagation in the Stern-Gerlach device: STA device (solid purple line) and the standard Stern-Gerlach apparatus with a magnetic field of modulus B_{av} (dotted purple line), B_{max} (dash-dotted purple line), and B_{st}^0 (dotted red line). Purple lines represent the use of equivalent resources in terms of magnetic field, while the dotted red line corresponds to a stronger magnetic field B_{st}^0 . The inset gives a logarithmic plot of the error committed $\epsilon(t) = 1 - \mathcal{F}(t)$ in the quantum state transfer for times t in the vicinity of the reference time $T = 2 \mu s$. The magnetic fields correspond to the parameters in Fig. 2.

$|\Delta t/T| \leq 2 \times 10^{-3}$, $\epsilon(t) \leq 10^{-5}$ for $|\Delta t/T| \leq 1.5 \times 10^{-2}$, and $\epsilon(t) \leq 10^{-2}$ for $|\Delta t/T| \leq 0.1$.

Equivalently, these fidelities can be achieved for a certain velocity interval $\Delta v = v - v_0$ around a reference velocity v_0 for which the STA magnetic field has been designed. The resilience of the STA and standard Stern-Gerlach devices increases with the strength of the magnetic field involved. With a maximum magnetic field of $B_{max} = 0.22$ G, the STA Stern-Gerlach achieves a fidelity $\mathcal{F} \geq 99\%$ for a class of velocities Δv such that $|\Delta v/v_0| \leq 10\%$. This corresponds to a velocity spread of $\Delta v \simeq 1$ km/s for the experiments [5,36] or for the slow beams of metastable hydrogen obtained from molecular dissociation in [28,29] or $\Delta v \simeq 4$ km/s for the fast hydrogen beams [27,29].

These measures can be compared with the reliability threshold for a universal set of quantum gates in order to obtain scalable quantum error correction [43–45]. As shown in these references, the availability of a finite set of gates enabling universal quantum computation with a probability of failure below a certain threshold indeed enables one to implement large-scale quantum error correction. The exact value of this threshold depends on a variety of factors such as the structure of the code employed and on the noise model [46]. Earlier estimates of this threshold gave a maximum failure probability of $p \simeq 2 \times 10^{-5}$ [47] for seven-qubit codes. Using a different topology, surface-code quantum computing [48,49] enables efficient quantum computation with gates fidelities of $\mathcal{F} \geq 99\%$.

The Stern-Gerlach device enhanced by the STA technique may thus obtain the transfer of a single quantum state with a reliability over this threshold for a significant range of propagation times, suggesting that this apparatus could be used within a quantum computing architecture.

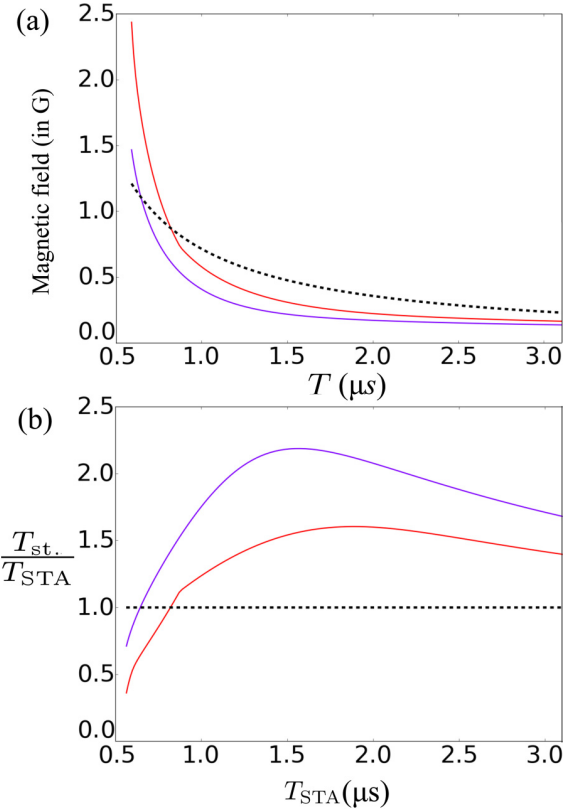


FIG. 5. (a) Maximum (solid red line) and average (solid purple line) magnetic fields used in a STA-engineered Stern-Gerlach device compared to the magnetic field in a standard Stern-Gerlach device (dotted black line) in order to perform an efficient spin transfer during the total time T . (b) Speed-up offered by the STA configuration: Ratio between the transfer times $T_{st.}$ required in a standard Stern-Gerlach device and T_{STA} required in a STA device versus the time T_{STA} . The standard Stern-Gerlach uses either a magnetic field of modulus B_{max} corresponding to the maximum field in the STA device (red line) or a magnetic field of modulus B_{av} corresponding to the average field in the STA device (purple line).

C. Speedup offered by the STA-engineered magnetic field

In order to evaluate quantitatively the benefits offered by the STA-engineered magnetic field over the standard helicoidal configuration, we estimate the resources, in terms of magnetic field, required to achieve a perfect spin transfer in a given total propagation time. As before, we consider either the average or the maximum magnetic field involved in the STA configuration to determine the equivalent magnetic field in the standard STA device. For a range of times T , we derive the STA-engineered magnetic field from Eq. (7), which gives readily the average and maximum magnetic fields involved. As seen previously, the magnetic field required in the standard device is inversely proportional to the propagation time T .

Figure 5 compares the performances of the STA-engineered and the standard Stern-Gerlach apparatuses from two equivalent points of views. Figure 5(a) shows magnetic field required in both devices for a range of atomic spin-transfer times T , while Figure 5(b) reveals the speedup offered by a STA Stern-Gerlach device in comparison with a standard

Stern-Gerlach device loaded with a magnetic field of similar strength. The figure reveals that for a total transfer time $T \gtrsim 0.8 \mu\text{s}$, the STA-engineered Stern-Gerlach device performs better. The maximum magnetic field involved in the STA device is smaller than the magnetic field required in a standard Stern-Gerlach device. Equivalently, the standard Stern-Gerlach device requires a longer atomic propagation time when using a magnetic field of modulus equal to the maximum STA magnetic field. Note that the curves associated with the maximum magnetic field in the STA device present a slope discontinuity [50].

On the other hand, when the atomic spin-transfer time is such that $T \lesssim 0.8 \mu\text{s}$, the standard Stern-Gerlach device becomes more efficient. Indeed, close to $T = 0.5 \mu\text{s}$, the magnetic field involved in the STA device diverges. This issue is related to the divergences generated by the roots of the angular functions $\theta(t)$ and $\phi(t)$, which appear in the interval $]0, T[$ when T goes below a certain value. By using polynomial functions of higher order, it is possible to go to shorter times while preserving a small enough magnetic field. When considering a family of polynomials of a given order, these divergences set a lower bound on the times achievable by the STA-engineered Stern-Gerlach devices.

To conclude, we have proposed to enhance the performances of a Stern-Gerlach device by using the technique of shortcut to adiabaticity. We have considered the propagation of spin-1 particles in the device. Using the Lewis-Riesenfeld invariant approach, we have found a suitable magnetic field

by reverse engineering the dynamical equation of motion for the invariant. The commutation between the invariant pointer and the Hamiltonian at initial and final times reduces the sensibility of the final state to the total propagation time. Using numerical simulations, we have demonstrated the validity of our approach and provided a quantitative picture of the enhancement offered by this technique. The STA-engineered Stern-Gerlach apparatus appears to offer a better trade-off between time of propagation and magnetic field involved in the device. This conclusion is generic and valid for higher angular momentum. It provides the physical limits for the miniaturization of a Stern-Gerlach device to entangle external and internal degrees of freedom. Finally, the STA-engineered Stern-Gerlach apparatus may achieve, for the transfer of a single atomic spin, extremely high fidelities for a narrow range of velocities and fidelities above 99% over a broad range of velocities. Such fidelities are below the error threshold for scalable quantum computation with surface codes. The fidelity enhancement provided by the STA method may open the possibility to use Stern-Gerlach devices in the context of quantum information processing.

ACKNOWLEDGMENT

F.I. acknowledges a very fruitful collaboration and enlightening discussions on atom optics and Stern-Gerlach interferometry with C. Renato de Carvalho, G. Jalbert, and N. Velho de Castro Faria.

-
- [1] O. Stern, *Z. Phys.* **7**, 249 (1921).
 - [2] J. Robert, C. Miniatura, S. L. Boiteux, J. Reinhardt, V. Bocvarski, and J. Baudon, *Europhys. Lett.* **16**, 29 (1991).
 - [3] M. V. Berry, *Proc. R. Soc. London A* **392**, 45 (1984).
 - [4] C. Miniatura, J. Robert, O. Gorceix, V. Lorent, S. Le Boiteux, J. Reinhardt, and J. Baudon, *Phys. Rev. Lett.* **69**, 261 (1992).
 - [5] C. Miniatura, J. Robert, S. L. Boiteux, J. Reinhardt, and J. Baudon, *Appl. Phys. B* **54**, 347 (1992).
 - [6] E. Torrontegui, S. Ibanez, S. Martínez-Garaot, M. Modugno, A. del Campo, D. Guéry-Odelin, A. Ruschhaupt, X. Chen, and J. G. Muga, *Adv. At. Mol. Opt. Phys.* **62**, 117 (2013).
 - [7] H. R. Lewis and W. B. Riesenfeld, *J. Math. Phys.* **10**, 1458 (1969).
 - [8] X. Chen, A. Ruschhaupt, S. Schmidt, A. del Campo, D. Guéry-Odelin, and J. G. Muga, *Phys. Rev. Lett.* **104**, 063002 (2010).
 - [9] A. Ruschhaupt, X. Chen, D. Alonso, and J. G. Muga, *New J. Phys.* **14**, 093040 (2012).
 - [10] A. Couvert, T. Kawalec, G. Reinaudi, and D. Guéry-Odelin, *Europhys. Lett.* **83**, 13001 (2008).
 - [11] R. Bowler, J. Gaebler, Y. Lin, T. R. Tan, D. Hanneke, J. D. Jost, J. P. Home, D. Leibfried, and D. J. Wineland, *Phys. Rev. Lett.* **109**, 080502 (2012).
 - [12] A. Walther, F. Ziesel, T. Ruster, S. T. Dawkins, K. Ott, M. Hettrich, K. Singer, F. Schmidt-Kaler, and U. Poschinger, *Phys. Rev. Lett.* **109**, 080501 (2012).
 - [13] J.-F. Schaff, X.-L. Song, P. Vignolo, and G. Labeyrie, *Phys. Rev. A* **82**, 033430 (2010).
 - [14] J.-F. Schaff, X.-L. Song, P. Capuzzi, P. Vignolo, and G. Labeyrie, *Europhys. Lett.* **93**, 23001 (2011).
 - [15] W. Rohringer, D. Fischer, F. Steiner, I. E. Mazets, J. Schmiedmayer, and M. Trupke, *Sci. Rep.* **5**, 9820 (2015).
 - [16] S. Martínez-Garaot, E. Torrontegui, X. Chen, M. Modugno, D. Guéry-Odelin, S.-Y. Tseng, and J. G. Muga, *Phys. Rev. Lett.* **111**, 213001 (2013).
 - [17] S. Martínez-Garaot, M. Palmero, J. G. Muga, and D. Guéry-Odelin, *Phys. Rev. A* **94**, 063418 (2016).
 - [18] D. Guéry-Odelin, J. G. Muga, M. J. Ruiz-Montero, and E. Trizac, *Phys. Rev. Lett.* **112**, 180602 (2014).
 - [19] I. A. Martinez, A. Petrosyan, D. Guéry-Odelin, E. Trizac, and S. Ciliberto, *Nat. Phys.* **12**, 843 (2016).
 - [20] A. Le Cunuder, I. A. Martínez, A. Petrosyan, D. Guéry-Odelin, E. Trizac, and S. Ciliberto, *Appl. Phys. Lett.* **109**, 113502 (2016).
 - [21] M. G. Bason, M. Viteau, N. Malossi, P. Huillery, E. Arimondo, D. Ciampini, R. Fazio, V. Giovannetti, R. Mannella, and O. Morsch, *Nat. Phys.* **8**, 147 (2012).
 - [22] B. B. Zhou, A. Baksic, H. Ribeiro, C. G. Yale, F. J. Heremans, P. C. Jerger, A. Auer, G. Burkard, A. A. Clerk, and D. D. Awschalom, *Nat. Phys.* **13**, 330 (2017).
 - [23] F.-Y. Zhang, W.-L. Li, and Y. Xia, [arXiv:1703.07933](https://arxiv.org/abs/1703.07933).
 - [24] S.-Y. Tseng and X. Chen, *Opt. Lett.* **37**, 5118 (2012).
 - [25] S. Martínez-Garaot, S.-Y. Tseng, and J. G. Muga, *Opt. Lett.* **39**, 2306 (2014).
 - [26] G. D. Valle, G. Perozziello, and S. Longhi, *J. Opt.* **18**, 09LT03 (2016).
 - [27] A. Medina, G. Rahmat, C. R. de Carvalho, G. Jalbert, F. Zappa, R. F. Nascimento, R. Cireasa, N. Vanhaecke, I. F. Schneider, N. V. de Castro Faria *et al.*, *J. Phys. B* **44**, 215203 (2011).

- [28] A. Medina, G. Rahmat, G. Jalbert, R. Cireasa, F. Zappa, C. de Carvalho, N. de Castro Faria, and J. Robert, *Eur. Phys. J. D* **66**, 134 (2012).
- [29] J. Robert, F. Zappa, C. R. de Carvalho, G. Jalbert, R. F. Nascimento, A. Trimeche, O. Dulieu, A. Medina, C. Carvalho, and N. V. de Castro Faria, *Phys. Rev. Lett.* **111**, 183203 (2013).
- [30] C. R. de Carvalho, G. Jalbert, F. Impens, J. Robert, A. Medina, F. Zappa, and N. V. de Castro Faria, *Europhys. Lett.* **110**, 50001 (2015).
- [31] We consider here the nonrelativistic regime and neglect the variation of the magnetic field over the extension of the atomic wave packet.
- [32] J. R. Johansson, P. D. Nation, and F. Nori, *Comput. Phys. Commun.* **183**, 1760 (2012).
- [33] J. R. Johansson, P. D. Nation, and F. Nori, *Comput. Phys. Commun.* **184**, 1234 (2013).
- [34] R. Jozsa, *J. Mod. Opt.* **41**, 2315 (1994).
- [35] R. D. Hight, R. T. Robiscoe, and W. R. Thorson, *Phys. Rev. A* **15**, 1079 (1977).
- [36] R. D. Hight and R. T. Robiscoe, *Phys. Rev. A* **17**, 561 (1978).
- [37] J. Robert, C. Miniatura, O. Gorceix, S. L. Boiteux, V. Lorent, J. Reinhardt, and J. Baudon, *J. Phys. II* **2**, 601 (1992).
- [38] E. Torrontegui, S. Martínez-Garaot, and J. G. Muga, *Phys. Rev. A* **89**, 043408 (2014).
- [39] S. Martínez-Garaot, E. Torrontegui, X. Chen, and J. G. Muga, *Phys. Rev. A* **89**, 053408 (2014).
- [40] Q. Zhang, X. Chen, and D. Guéry-Odelin, [arXiv:1705.05164](https://arxiv.org/abs/1705.05164).
- [41] Note that one may construct a physical static magnetic field $\mathbf{B}(\mathbf{r})$ such that the function $\mathbf{B}(t)$ corresponds to the magnetic field seen by the atom in the nonrelativistic limit, i.e., $\mathbf{B}(t) = \mathbf{B}(\mathbf{r}(t))$, with $\mathbf{r}(t)$ being the particle position. Indeed, Eq. (2) constrains only the gradient of the magnetic field along the direction of the atomic motion. Other components of the magnetic field gradient may be chosen at will to ensure consistency with Maxwell equations.
- [42] At the final time the singularity arising from the cancellation $\varphi(T) = 0$ is cured by a simultaneous cancellation of the derivative $\dot{\varphi}(T) = 0$.
- [43] P. W. Shor, in *Proceedings of the 37th Annual Symposium on Foundations of Computer Science* (IEEE Computer Society Press, Washington, DC, 1996), pp. 56–65.
- [44] E. Knill, R. Laflamme, and W. H. Zurek, *Proc. R. Soc. London A* **454**, 365 (1998).
- [45] J. Preskill, *Proc. R. Soc. London A* **454**, 385 (1998).
- [46] D. Gottesman, [arXiv:0904.2557](https://arxiv.org/abs/0904.2557).
- [47] P. Aliferis, D. Gottesman, and J. Preskill, *Quantum Inf. Comput.* **6**, 97 (2006).
- [48] A. G. Fowler, M. Mariantoni, J. M. Martinis, and A. N. Cleland, *Phys. Rev. A* **86**, 032324 (2012).
- [49] R. Barends, J. Kelly, A. Megrant, A. Veitia, D. Sank, E. Jeffrey, T. C. White, J. Mutus, A. G. Fowler, B. Campbell *et al.*, *Nature (London)* **508**, 500 (2014).
- [50] A slope discontinuity occurs in Fig. 5 because the maximum magnetic field, namely, $B_{\max}(T) = \max\{\|\mathbf{B}(t, T)\| \mid t \in]0, T[\}$, is not a continuously differentiable function of T . The STA magnetic field, obtained through a reverse-engineering procedure depending on the total duration T , can be seen as a function of two variables $\mathbf{B}(t, T)$. Close to the singularity $T_S \simeq 0.8 \mu\text{s}$, the function $t \rightarrow \|\mathbf{B}(t, T)\|$ has two distinct local maxima in the interval $]0, T[$, associated with the instants $t_1(T)$ and $t_2(T)$ such that $t_1(T) < t_2(T)$. The profile of this function depends smoothly on the total time T . For the specific value $T = T_S$ these two local maxima are equal, i.e., $\|\mathbf{B}(t_1(T_S), T_S)\| = \|\mathbf{B}(t_2(T_S), T_S)\|$. For $T < T_S$ one has $\|\mathbf{B}(t_1(T), T)\| > \|\mathbf{B}(t_2(T), T)\|$ and thus $B_{\max}(T) = \|\mathbf{B}(t_1(T), T)\|$. For $T > T_S$, one has $B_{\max}(T) = \|\mathbf{B}(t_2(T), T)\|$. Since the difference $|t_1(T_S) - t_2(T_S)| > 0$ is finite, one obtains a slope discontinuity for $B_{\max}(T)$ in $T = T_S$. This also induces a slope discontinuity in the ratio $T_{\text{st.}}/T_{\text{STA}}$ associated with a standard Stern-Gerlach device using a field of modulus $B_{\max}(T_{\text{STA}})$.